André P. Mendes; Bruno Baptista
Marina S. Perdigão; André M. S. Mendes

EXPERIMENTAL ANALYSIS OF A DC CURRENT-CONTROLLED VARIABLE INDUCTOR IN A DC-DC CONVERTER

Abstract

This paper presents an analysis for the experimental set up of a double toroid variable inductor (VI) that is fed by a DC-DC converter. The main objective is to analyze the behaviour of the VI for different power levels, in particular the influence of the control circuit to regulate the inductance of the main winding. By observing the waveform of the main current winding, it is possible to demonstrate the ability to increase or decrease the inductance value. A variable inductor is typically used from linear to saturated state and presents an inversely proportional inductance as a function of the main winding current. By employing this current-controlled double toroid VI it is possible to have both an inductance increase and inductance decrease as a function of the control current by regulating the reluctance of the magnetic cores.

Index Terms—variable inductor, inductance, saturation, toroid, ripple control.

1 Introduction

A variable inductor (VI) is a device that changes the inductance of a winding when the permeability of a magnetic core is regulated. The permeability of the magnetic core can be changed through a control current that will introduce a DC magnetic flux on the core [1]–[9].

Common applications for this device are: reactive power control [9], LED lighting and correspondent driver's control [7], [8], [10], [11], power factor correction [12] and current ripple reduction [13]. Laboratory experiments with VIs have been done with different magnetic core designs, in particular the double E [11], [12], [14], triple E [8] and toroid core design [3], [6], [13], [15]. The research done on the double toroid type has not explained its behaviour for different power levels. In particular, the way the inductance as a function of the control current changes.

The following paper describes the VI operation with a double toroid configuration on an experimental setup, with a focus on the analysis of the main winding inductance as a function of the control current. This relationship is important when the VI is projected, because it shows the maximum and minimum values of the inductance for different states of saturation on the magnetic material.

The paper is organized in four sections. The introduction gives a brief definition of the VI operation and its applications with a focus on the experimental research. Section II describes the system's operation, parameterization and calculations to be done for the experimental analysis. Section III shows the experimental setup and results with a thorough explanation of the system behaviour. Finally, section IV concludes the work presented in this paper.

II. System description

The experimental tests were conducted with a DC-DC buck converter that is shown in Fig. 1.

The DC bus link is obtained through a rectifier circuit from the AC voltage of the grid. The input voltage is regulated with an autotransformer. This circuit is adapted from an inverter configuration, in which only one arm is used. During T_{on} of Q1 $_{imain}$ increases linearly and the voltage at the terminals of L_{main} is given by $V_{DClink} - V_{Load}$.

When Q1 is switched off only D2 conducts and the voltage on L_{main} is given by $-V_{Load}$, therefore the current will decrease linearly. The IGBT Q2 is turned off at all times. In order to guarantee that no current goes into the DC link, a diode D_{link} is connected in series with the DC link, as shown in Fig. 1.

The capacitor C_{load} is chosen in order to obtain a constant DC voltage at R_{load}.

A control circuit capable of regulating the operating frequency (fs) allows modeling the duty cycle Ds from 0 to 80% and fs up to 25 kHz. The control circuit was implemented on a digital signal processor capable of generating the voltage pulses for the semiconductors.

There are two main ways of operating the double toroid variable inductor:

- One core has opposing magnetic flux and the other has adding magnetic flux, marked by the blue and orange arrows in both cores in Fig. 2a (configuration A);
- Both cores having opposing magnetic flux, marked by the blue and orange arrows in both cores in Fig. 2b (configuration B).

The main drawback of operating the VI with configuration B, shown in Fig. 2b, is that the induced voltages on the control windings do not cancel each other out. This causes high voltages to appear at the terminals of the control current source, which can damage it. For that reason, this configuration is not considered for this work. On the other hand, the configuration A, shown in Fig. 2a, enables the variation of the main inductance at the expense of one core getting saturated.

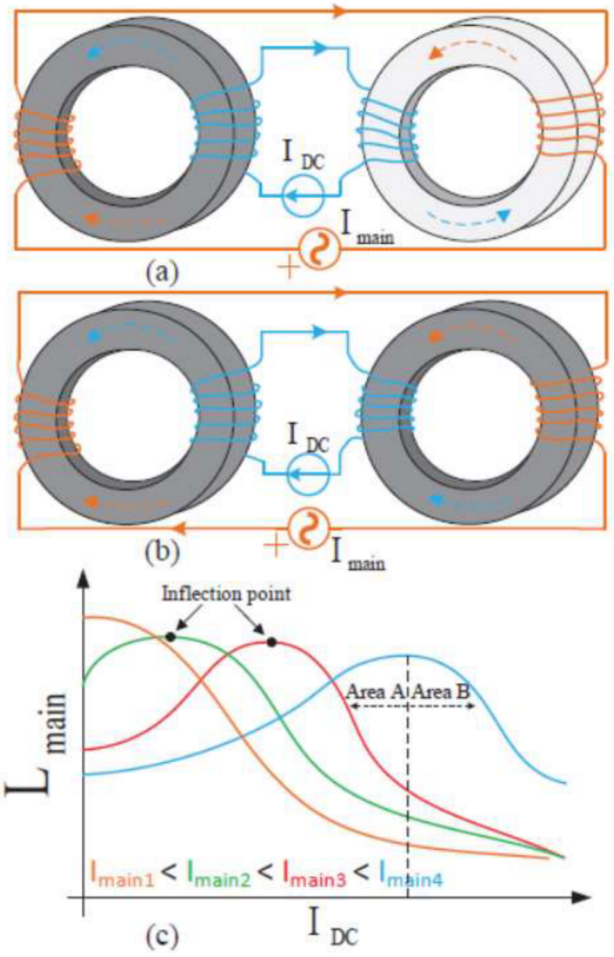

Fig. 2: Design and characteristic of the double toroid VI: (a) Configuration A; (b) Configuration B; (c) Characteristic curve for different Imain values

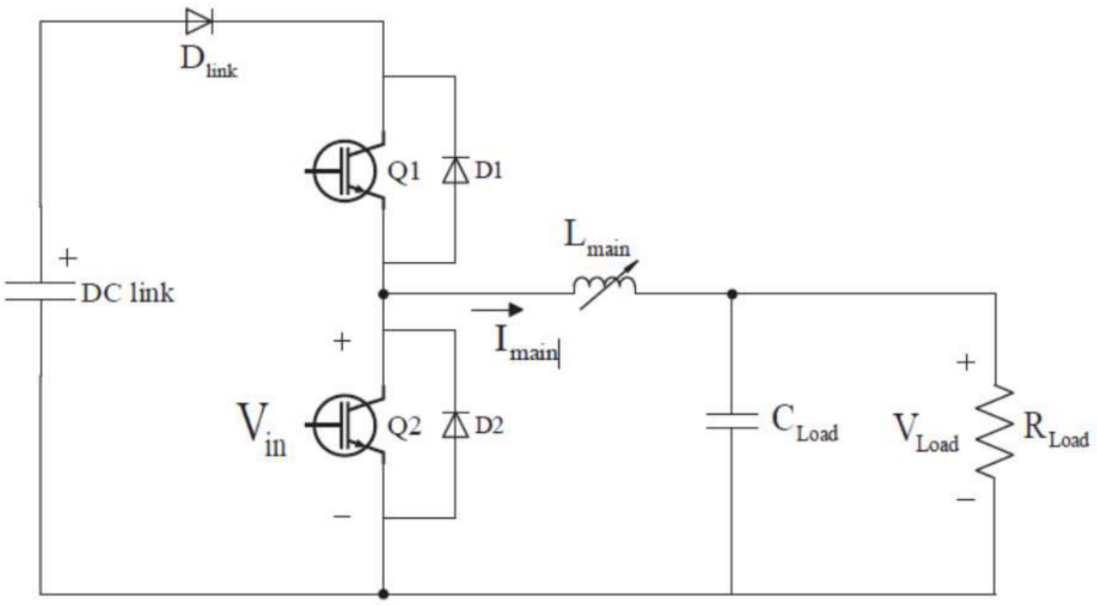

Fig. 1: Schematic diagram for the DC-DC buck converter with the VI and load

Table I displays the different values and characteristics of the components used in this system. The values obtained for the VI windings, Cload and Rload were measured using an LCR meter at 10 kHz, which is the closest frequency setting available, compared to the frequency of operation (20 kHz).

As for the duty cycle, a value of 80% was chosen in order to guarantee that critical conduction is avoided. The core height is equivalent to two cores stacked, so each core is composed of two N87 cores. The control current source has limitations and can only output up to 3.2 A, therefore an higher number of turns is used on the control windings in order to obtain high magnetomotive force FDC with low DC current. The main and control windings are composed of two windings connected in series. N_{main} and $N_{control}$ refer to one winding.

Knowing that the design chosen is represented by configuration A, the operation of the VI works as follows: The VI is fed with a main current that will create a magnetic flux named ϕ_{main}. As a result, only magnetomotive force F_{main} will be present. By powering the control windings with some DC current, FDC will exist and contribute to the existing m.m.f. on the right core (adding), while counteract on the other core (cancelling). As such, there will be a point in the left core where the resultant m.m.f. F_{total} is approximately zero

TABLE I: Variables of the magnetic and electric components

Properties and parameters			
Core type	Toroid (N87)	$ESR_{1control}$	26.9 Ω
Dimensions	102x68x31.3 mm	$ESR_{2control}$	30.8 Ω
N_{main}	26	**DC link**	0-100 V
$N_{control}$	179	f_s	0-25 kHz
ESR_{1main}	1.58 Ω	C_{load}	1 mF
ESR_{2main}	1.69 Ω	R_{load}	7 Ω

In that point of operation, which is defined as the inflection point, $F_{main} = F_{DC}$. Fig. 2c shows the inductance behavior of the main winding ($L_{1main} + L_{2main}$) as a function of the control current, where the specific points of inflection are noted for different characteristic curves. It is important to note that depending on the average value of i_{main}, a certain F_{main} will exist.

Higher values of I_{main} will require more control current to cancel that F_{main}, hence why the inflection point travels to the right with higher values of I_{main}. It is also evident that the inductance presents two main characteristics as shown in Fig. 2c: an increase in L_{main} with an increase in IDC and a decrease in L_{main} with an increase in IDC. Depending on the state of operation of the VI only one or two of these characteristics are available. The blue curve on Fig. 2c has both areas highlighted. Area A to the left of the inflection point and area B to the right of the inflection point. For that curve, area A is greater than area B and if a different combination is needed, only I_{main} needs to be changed. The green curve will have, approximately, the same maximum inductance value but at a smaller control current and area B will be higher than area A. For a specific application it is important to select the desired behaviour.

Inductance calculation

Several formulas can be used to compute the inductance of the main winding. It is, however, difficult to obtain in an experimental setup several variables. One of such, is the relative permeability μr at a certain point of operation of the magnetic material. Nevertheless, equations (1) and (2) are important to explain the relationship between the inductance and the relative permeability.

$$\Re = \frac{\ell}{\mu A} \tag{1}$$

with μ = μ0μr and the inductance is calculated through

$$L = \frac{N^2}{\Re} \tag{2}$$

on another note, the formula of the inductance from the DCDC buck converter is defined by equation (3)

$$L_{main} = \frac{(V_{DClink} - V_{load}) D_s T_s}{\Delta i_{main}} \tag{3}$$

where Ds is the duty cycle, Ts is the period of operation and Δi_{main} is the main current ripple.

With this equation the calculation of the main inductance can be done for all values of IDC and is not dependent on the magnetic properties of the cores. Analysis of this equation shows that a high ripple translates into a lower inductance, while a small ripple means that a higher inductance is obtained. The frequency of operation and the duty cycle are constant for the experiment, therefore their values are not relevant for the variability of the main winding inductance.

Since a low value of inductance equates to a high ripple, it is possible to state that a high current ripple happens when the magnetic cores are saturated, i.e. the permeability on them is small as highlighted by (1) and (2). Conversely, a high inductance equates to a high permeability on the magnetic cores, which in this case will only be possible on the left core (Fig. 2a), because of the opposing fluxes. The right core will saturate due to the adding fluxes.

The ripple value will be used as a way to visually interpret when the maximum and minimum inductances are reached and to identify operation on areas A and B.

III. Experimental setup and results

The experimental setup is pictured in Fig. 3 and displays all the components used. The digital signal processor (TMS320F28335 from TI) is used in order to generate the pulses for IGBT Q1 (SEMIX202GB066HDS) and to control the frequency and duty cycle of the system. The interface board computes the signals given from the DSP and injects them in the IGBT's driver (SKYPER 32 PRO). A DC voltage source (PSM2/2A) is needed as an external power source to this board. The control current source (GS610 from Yokogawa), under the DC voltage source, is connected to the control windings.

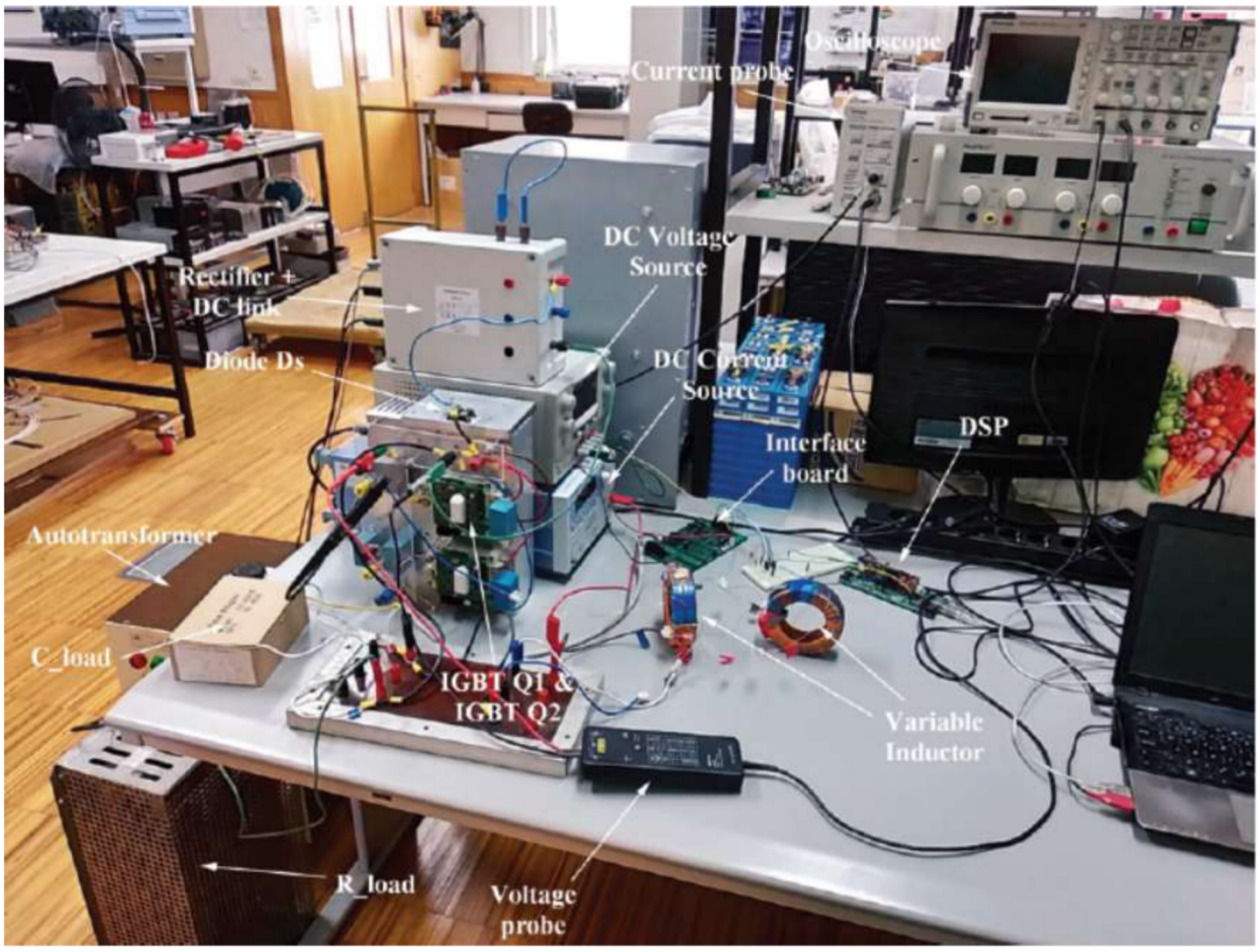

Fig. 3: Overview of the experimental setup

The results taken from the oscilloscope were obtained through WaveStar for Oscilloscopes by importing the data to a laptop. A detailed look over the variable inductor is displayed on Fig. 4. The magnetic cores are visible, each with two N87 cores stacked. Furthermore, the main and control windings are identified and it is clear the difference in the number of turns used.

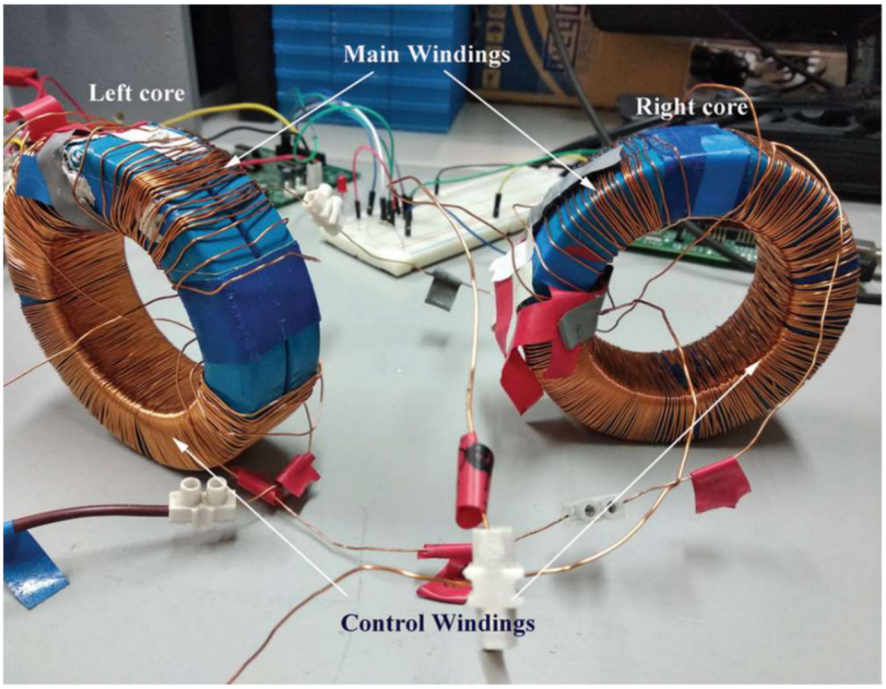

Fig. 4: Close look over the two toroids

Two main experimental tests were considered: one with a value of i_{main_avg} of around 4.2 A and other with a value of 7.3 A.

This way it is possible to obtain two characteristic curves in two different states of operation. The initial test depicts the operation of a VI with standard conditions in which the inductance decreases with the increase in control current. The second test has an higher i_{main_avg} and shows the new behaviour of the inductance when the control current is changed. For this case the inductance increases until a maximum value is reached and then decreases again as the control current is further incremented.

A. Operating current i_{main_avg} = 4.2 A

A first experimental test was performed to show the behavior of the double toroid VI on a state of operation characterized by a low value of i_{main_avg}. This current is obtained by regulating the DC link voltage to 40 V. Table II shows the data obtained for a control current between 0 and 2 A. The average current on the main winding as well as ripple values Δi_{main} are taken directly from the oscilloscope readings. V_{load} is obtained with a multimeter because it allows for better precision at different IDC levels.

TABLE II: Experimental data for VDClink = 40 V

I_{DC}	i_{main_avg}	Δi_{main}	V_{load}	L_{main} (mH)
0	4,18	1,12	27,8	0,4357
0,1	4,18	1,19	28	0,4034
0,2	4,18	1,26	28	0,381
0,3	4,2	1,34	28	0,3582
0,4	4,12	1,42	28,1	0,3352
0,5	4,16	1,54	28,2	0,3065
0,6	4,11	1,66	28,15	0,2855
0,7	4,14	1,84	28,1	0,2587
0,8	4,14	2	28,1	0,238
0,9	4,13	2,12	28,1	0,2245
1	4,18	2,26	28,1	0,2106
1,1	4,2	2,46	28	0,1951
1,2	4,2	2,52	28,05	0,1897
1,3	4,22	2,58	28,1	0,1845
1,4	4,18	2,68	28,05	0,1783
1,5	4,13	2,8	28	0,1714
1,6	4,12	2,84	28,2	0,1662
1,7	4,13	2,86	28	0,1678
1,8	4,12	2,94	28	0,1633
1,9	4,11	2,96	28	0,1622
2	4,11	3,06	27,9	0,1582

The average value for the main current stays relatively constant, despite the increase in control current. Moreover, the voltage at the terminals of the load is also unaffected by the increase in DC current.

The peak to peak value of the main current was registered for all the values of DC current and it is clear that in this experiment an higher DC current leads to higher ripple. The waveform representation of i_{main} for three values of IDC at 0, 0.5 and 1 A is shown on Fig. 5a and this increase is clearly visible. At IDC = 0 A the ripple value amounts to only 26.8% of i_{main_avg}. With IDC = 2 A the ripple accounts for 74.5% of the main current value. An higher ripple value will be responsible for higher losses on the system, particularly in the magnetic core. Moreover, induced voltages on the control windings are proportional to the rate of change of the magnetic flux. If the ripple increases, this rate of change will also increase. One of the great advantages of the VI implementation is the ability to control this effect and maintain the power current with minimum ripple. Fig. 5b shows the effect of the induced voltages on the control winding circuit. Even though the DC current source outputs a constant current, its waveform is affected by the voltage reflections on the control circuit. As previously stated, the design chosen of Fig. 2a cancels the induced voltages on the control windings, albeit not completely. Therefore, these induced voltages cause the control current to have a triangular shape, similar to the one on the power circuit.

The rightmost column of Table II displays the inductance of the main winding. Its calculation is done with (3). The only variable that changes is the ripple, therefore as the ripple increases the inductance decreases. This behaviour is plotted on Fig. 6 which shows the inductance as a function of the control current. The inflection point does not appear on this curve and the maximum inductance is obtained when no control current is injected. Therefore, this state of operation is relative to a characteristic curve that only has the B operation area behaviour, as shown in Fig. 2c (orange curve). In order to explain the reason for this behaviour it is important to look at Fig. 2a. The right core will be always saturated because both fluxes add each other. Without control current both cores have a magnetomotive force F_{main}. When the control circuit is activated the left core has a total magnetomotive force given by equation (4).

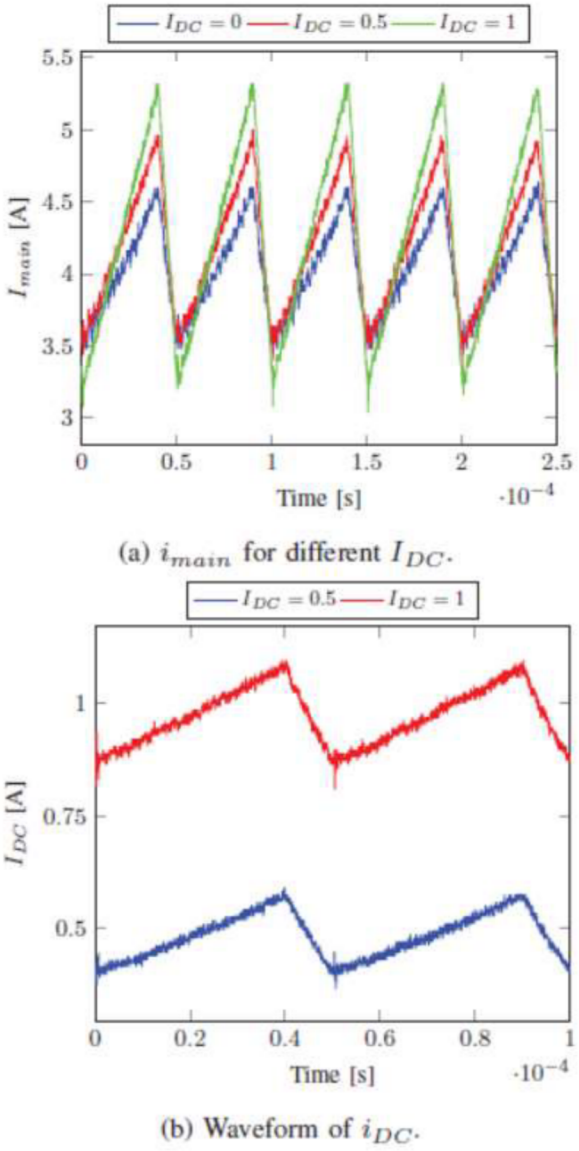

Fig. 5: Waveforms of i_{main} and i_{DC} for V_{DClink} = 40 V

$$F_{total} = F_{main} - F_{DC} \quad (4)$$

The left core has an initial saturation state due to I_{main}. However, the graphical representation on Fig. 6 shows that both cores saturate when the control current rises, which can be concluded by seeing that the inductance is always decreasing. This is attributed to the fact that the left core starts to saturate due to the DC flux. In that sense, the initial value of F_{main} is small enough so that FDC at IDC = 0.1 A is much higher than Fmain in this point of operation.

For small values of operating current in the main windings, the inflection point is not visible and the left core saturates due to the DC flux. An application that requires lowering the inductance with an increase in control current needs to have this kind of characteristic. The implementation of this kind of VI is not very efficient due to the need to saturate the cores even further to get those results, which causes further losses in the system.

B. **Operating current i_{main_avg} = 7.3 A**

The second experimental test involves, as shown in Table III, the increase of the DC link voltage from 40 V to 70 V.

By increasing this voltage, the average current i_{main_avg} will increase and put the magnetic cores with a saturation level higher than the previous test.

Similarly to the initial experiment, the average current and the voltage at the load remain stable throughout the change in IDC. The ripple value has a maximum value at IDC = 0 A and reaches its minimum value at IDC = 0.9 A, when the left core is unsaturated. Fig. 7a shows the difference between i_{main} waveforms with three IDC values. The ripple decreases until IDC = 0.9 A and then increases again for higher DC control currents. The three waveforms are relative to control currents of 0, 1 and 2 A. It is also important to note that the higher the value of i_{main_avg} the higher will be Δi_{main}.

Without DC flux present, the ripple accounts for 108% of the average value and is reduced significantly to 54% with a control current of 1 A. In terms of experimental observation it was possible to know when the inductance was increasing or decreasing by observing the ripple variation. In addition, the waveforms on Fig. 7a show that under higher core saturation, i_{main} presents a non linear characteristic that is seen on the blue waveform. With IDC = 1 A the red waveform has a more linear behaviour. The two control current waveforms shown in Fig. 7b are more or less equivalent to the ones shown in Fig. 5b with the only difference being the constant values considered for this case (1 and 2 A).

TABLE III: Experimental data for V_{DClink} = 70 V

$I_{control}$	I_{main}	Δi_{main}	V_{load}	L_{main} (mH)
0	7,33	7,92	48,7	0,1076
0,1	7,37	7,76	48,6	0,1103
0,2	7,38	7,6	48,7	0,1121
0,3	7,38	7,44	48,7	0,1145
0,4	7,34	6,64	48,7	0,1283
0,5	7,27	6,24	48,6	0,1372
0,6	7,32	5,04	48,7	0,1690
0,7	7,37	4,64	48,6	0,1845
0,8	7,33	3,68	48,6	0,2326
0,9	7,33	3,44	48,6	0,2488
1	7,33	4	48,6	0,214
1,1	7,36	4,08	48,7	0,2088
1,2	7,35	4,4	48,6	0,1945
1,3	7,37	4,48	48,7	0,1901
1,4	7,35	4,64	48,7	0,1836
1,5	7,31	4,8	48,7	0,1775
1,6	7,28	5,04	48,7	0,1690
1,7	7,29	5,2	48,7	0,1638
1,8	7,34	5,52	48,7	0,1543
1,9	7,26	5,6	48,7	0,1521
2	7,36	5,81	48,8	0,1459

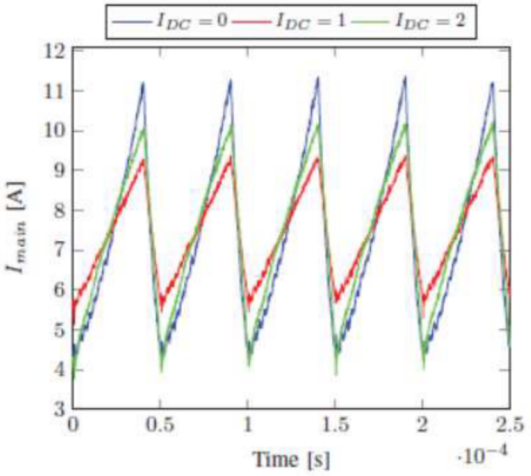

(a) i_{main} for different I_{DC}.

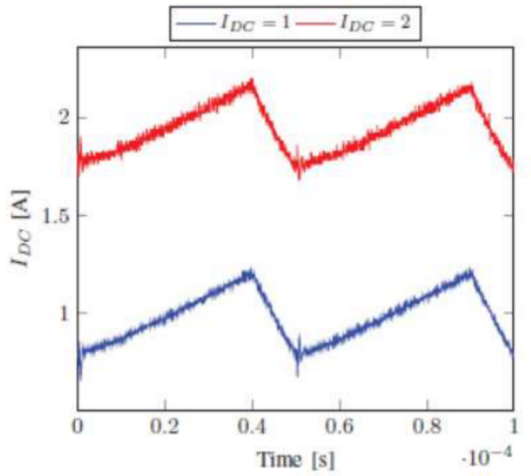

(b) Waveform of i_{DC}.

Fig. 7: Waveforms of i_{main} and i_{DC} for V_{DClink} = 70 V

It is known that the initial saturation state of both cores is higher than before, as such their permeability is smaller. Moreover, F_{main} is also higher and to cancel it on the left core, more control current is needed. Indeed, by following the same thought process with (4), it is possible to conclude that the inflection point will occur due to the higher magnitude of main flux. The first values of control current reduce the saturation on the left core, increasing its permeability and therefore the inductance, as depicted in Fig. 8. At some point $F_{main} \approx F_{DC}$ and the inductance reaches a maximum value due to the maximum permeability, which in this case happens at around I_{DC} = 0.9 A. If the control current is further increased, the left magnetic core will start to saturate again but this time due to the DC flux. The ripple of i_{main} will increase again and the inductance gets smaller. The plot of Fig. 8, that is made with the values from Table III summarizes this behaviour. This curve displays both operation areas A and B that were referred in Fig. 2c. On area A $F_{main} > F_{DC}$ whereas on area B $F_{main} < F_{DC}$.

These two experiments show the behaviour of the inductance curves when the main current is increased, i.e. its shift to the right, as pictured in the curves of Fig. 2c. The results of the first experiment shown in Fig. 6 allow for a variation only on area B, while the results of the second experiment regulate the VI on both areas, as illustrated in Fig. 8. The orange curve with only area B and the red curve with both areas, shown in Fig. 2c, have a similar representation to the ones obtained experimentally, as can be observed in Fig. 6 and Fig. 8. It is also important to note the difference on the inductance variation on Fig. 6 and Fig. 8: the first experiment has a variation of 175% relative to the minimum value, whereas on the second test the variation is 131%. Considering that the i_{main} ripple on the second test is higher it is possible to conclude that the magnetic cores on the second test are more saturated, so the variation of inductance that can occur is more limited.

IV. Conclusion

This work provides a study of a double toroid operation under experimental test conditions.

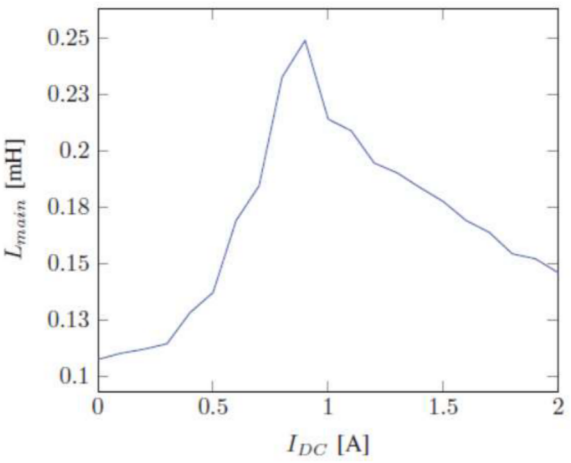

Fig. 8: L_{main} as a function of IDC for V_{DClink} = 70 V

A prototype, based on a DC-DC Buck converter, was built and data was retrieved in order to analyze the VI operation. Brief considerations regarding the applicability of the VI are made. The system description and parameterization is also addressed.

Two experimental tests were done to display the operation of the VI under two different modes. The first test with a small I_{main} shows an inductance behaviour in which both cores are lightly saturated by the main magnetic flux, as seen by the small ripple values. In this test, a small control current is enough to saturate the left core due to the high number of turns, producing a dominant DC flux. Consequently, the saturation level will be caused by FDC not allowing the observation of the inflection point. Increasing the control current will saturate both cores even more, one due to the DC flux and the other due to both fluxes. Therefore, the inductance will only display the behaviour shown by operation area B in Fig. 2c, i.e. decreases with the increase in DC current. The second test with a higher I_{main} increases the F_{main} and for that reason more DC current is necessary to generate an opposing FDC, in order to obtain the maximum inductance value. From this point there are two options to decrease the inductance, which is done by increasing or decreasing the DC current. Despite having the same inductance values, operating on area A results in less Joule losses in the control windings.

Observing the ripple in the current waveforms on the main windings is enough to understand when the inductance is rising or decreasing, by watching its value decrease or increase, respectively.

References

[1] R. Hooper, B. Guy and R. Perrault, "A current-controlled variable inductor," in IEEE Instrumentation & Measurement Magazine, vol. 14, no. 4, pp. 39-44, Aug. 2011.

[2] J. M. Alonso, M. Perdigão, M. A. Dalla Costa, S. Zhang and Y. Wang, "Variable inductor modeling revisited: The analytical approach," 2017 IEEE Energy Conversion Congress and Exposition (ECCE), Cincinnati, OH, 2017, pp. 895-902.

[3] M. W. Beraki, J. P. F. Trovão, M. S. Perdigão and M. R. Dubois, "Variable Inductor Based Bidirectional DC–DC Converter for Electric Vehicles," in IEEE Transactions on Vehicular Technology, vol. 66, no. 10, pp. 8764-8772, Oct. 2017.

[4] J. M. Alonso, M. S. Perdigão, G. Z. Abdelmessih, M. A. Dalla Costa and Y. Wang, "SPICE Modeling of Variable Inductors and Its Application to Single Inductor LED Driver Design," in IEEE Transactions on Industrial Electronics, vol. 64, no. 7, pp. 5894-5903, July 2017.

[5] S. M. Ahsanuzzaman, T. McRae, M. M. Peretz and A. Prodi´c, "Lowvolume buck converter with adaptive inductor core biasing," 2012 Twenty-Seventh Annual IEEE Applied Power Electronics Conference and Exposition (APEC), Orlando, FL, 2012, pp. 335-339.

[6] M. S. Perdigão, J. P. F. Trovão, J. M. Alonso and E. S. Saraiva, "Large-Signal Characterization of Power Inductors in EV Bidirectional DC–DC Converters Focused on Core Size Optimization," in IEEE Transactions on Industrial Electronics, vol. 62, no. 5, pp. 3042-3051, May 2015.

[7] M. S. Perdigão, M. F. Menke, Á. R. Seidel, R. A. Pinto and J. M. Alonso, "A Review on Variable Inductors and Variable Transformers: Applications to Lighting Drivers," in IEEE Transactions on Industry Applications, vol. 52, no. 1, pp. 531-547, Jan.-Feb. 2016.

[8] E. A. Bitencourt, M. R. Cosetin, I. G. Vegner and R. N. do Prado, "A ferromagnetic based variable inductor analysis and design methodology," 2015 IEEE 13th Brazilian Power Electronics Conference and 1st Southern Power Electronics Conference (COBEP/SPEC), Fortaleza, 2015, pp. 1-5.

[9] K. Nakamura et al., "Development of Concentric-Winding Type Three-Phase Variable Inductor," in IEEE Transactions on Magnetics, vol. 51, no. 11, pp. 1-4, Nov. 2015.

[10] Y. Hu, L. Huber and M. M. Jovanovi´c, "Universal-input single-stage PFC flyback with variable boost inductance for high-brightness LED applications," 2010 Twenty-Fifth Annual IEEE Applied Power Electronics Conference and Exposition (APEC), Palm Springs, CA, 2010, pp. 203-209.

[11] M. Martins, M. S. Perdigão, A. M. S. Mendes, R. A. Pinto and J. M. Alonso, "Analysis, Design, and Experimentation of a Dimmable Resonant-Switched-Capacitor LED Driver With Variable Inductor Control," in IEEE Transactions on Power Electronics, vol. 32, no. 4, pp. 3051-3062, April 2017.

[12] Cheon-Yong Lim, J. H. Kim, Yeonho Jeong, Dong-Kwan Kim, Han-Shin Youn and Gun Woo Moon, "A high efficiency critical mode boost PFC using a variable inductor," 2016 IEEE 8th International Power Electronics and Motion Control Conference (IPEMC-ECCE Asia), Hefei, 2016, pp. 2792-2797.

[13] Y. Gu, D. Zhang and Z. Zhao, "Input Current Ripple Cancellation Technique for Boost Converter Using Tapped Inductor," in IEEE Transactions on Industrial Electronics, vol. 61, no. 10, pp. 5323-5333, Oct.2014.

[14] R. A. Pinto, J. M. Alonso, M. S. Perdigão, M. F. da Silva and R. N. do Prado, "A New Technique to Equalize Branch Currents in Multiarray LED Lamps Based on Variable Inductors," in IEEE Transactions on Industry Applications, vol. 52, no. 1, pp. 521-530, Jan.-Feb. 2016.

[15] M. Beraki, M. Perdigao, F. Machado and J. P. Trovão, "Auxiliary converter for variable inductor control in a DC-DC converter application," 2016 51st International Universities Power Engineering Conference (UPEC), Coimbra, 2016, pp. 1-6.